


## Effect of size on the thermal noise and acoustic response of viscous-driven microbeams

Junpeng Lai,<sup>1,a)</sup>  Mahdi Farahikia,<sup>2</sup> Morteza Karimi,<sup>1</sup>  Zihan Liu,<sup>1</sup>  Yingchun Jiang,<sup>1</sup>  Changhong Ke,<sup>1</sup>   
 and Ronald Miles<sup>1,b)</sup> 

<sup>1</sup>Department of Mechanical Engineering, Binghamton University, Binghamton, New York 13902, USA

<sup>2</sup>Division of Engineering Programs, State University of New York at New Paltz, New Paltz, New York 12561, USA

### ABSTRACT:

A study is presented of the thermal-mechanical noise and response to sound of microphones that are designed to be driven by the viscous forces in air rather than by sound pressure. Virtually all existing microphone designs are intended to respond to sound pressure. The structures examined here consist of thin, micro-scale, cantilever beams. The viscous forces that drive the beams are proportional to the relative velocity between the beams and fluid medium. The beams' movement in response to sound is similar to that of the air in a plane acoustic wave. The thermal-mechanical noise of these beams is found to be a very weak function of their width and length; the size of the sensing structure does not appear to significantly affect the performance. This differs from the well-known importance of the size of a pressure-sensing microphone in determining the pressure-referred noise floor. Creating microphones that sense fluid motion rather than pressure could enable a significant reduction in the size of the sensing element. Calculated results are revealed to be in excellent agreement with the measured pressure-referred thermal noise. © 2024 Acoustical Society of America. <https://doi.org/10.1121/10.0025546>

(Received 3 January 2024; revised 12 March 2024; accepted 22 March 2024; published online 10 April 2024)

[Editor: Robert D. White]

Pages: 2561–2576

### I. INTRODUCTION

When any microphone is used to detect low-level sounds, its output signal can be significantly influenced by unwanted noise. This noise can be introduced in the electronic circuit or it could be due to thermal-mechanical motion of the pressure-sensing diaphragm. Whereas future advances in circuit design may reduce the electronic noise, there are currently few options for designers to reduce thermal-mechanical noise. To reduce thermal-mechanical noise in pressure-sensing microphones, designers have only two options: (1) reduce viscous damping and/or (2) increase the diaphragm area (Gabrielson, 1993; Miles, 2020). The pursuit of either of these options can adversely impact production costs and other performance metrics.

The reduction of thermal noise in the output signal can be particularly vexing in microphones fabricated using the technology of micro-electromechanical systems (MEMS) microphones, which tend to be more susceptible to thermal noise than other, larger microphones. MEMS microphones have revolutionized the microphone industry and are incorporated in billions of electronic products. Because the cost of these devices is strongly influenced by their size and, hence, the number of them that can be produced on each silicon wafer, there is enormous pressure to minimize the size of each design.

One approach to this challenge could be to consider a microphone design that is based on sensing the fluid motion

in a sound field rather than the pressure. This would be a radical departure from the usual microphone design approach, which, with almost no exceptions, has always been about the measurement of sound pressure. It has been argued (Fellgett, 1987) that the fundamental limits on the size of a velocity sensing microphone could be quite different than that for a pressure-sensing microphone.

Even so-called “velocity” microphones, such as the ribbon microphone (Julius and Olson, 1932), are based on detecting pressure differences on each side of a thin ribbon rather than velocity. It could be argued that the ribbon microphone is actually a “pressure gradient” microphone as it is not driven directly by fluid velocity. The motion of the ribbon is a direct result of sound pressure. The driving force on the ribbon is similar to that of any pressure-sensing structure, such as a tympanic membrane or diaphragm, which, as Newton taught us, moves in response to the net difference (or gradient) in pressure on its opposite surfaces. Pressure gradients, of course, also result in motion of the fluid. Our interest here, however, is on structures that respond primarily to viscous forces caused by the relative velocity between the structure and surrounding fluid. Viscous forces are *not* generally believed to play a major role in the motion of pressure-sensing tympana or diaphragms or ribbon microphones but they are considered to be important in the flow-induced motion of thin hairs or cilia (Bezares-Calderón *et al.*, 2020; Tao and Yu, 2012).

It is not immediately clear whether sensing fluid velocity rather than pressure would lead to desirable performance and meet the design requirements of typical microphone

<sup>a)</sup>Email: jlai16@binghamton.edu

<sup>b)</sup>Email: miles@binghamton.edu

applications. It might, however, result in designs that avoid some of the current design roadblocks. This study is motivated by a desire to give the idea of sensing acoustic fluid velocity a more proper amount of consideration in microphone design.

The design of microphones that sense acoustic particle velocity has received scant attention relative to the extensive literature on pressure-sensing microphones. There have, however, been some notable advances. [Forbes \(1887\)](#) may have been the first to create a microphone that responded to the velocity of the air in a sound field. The device relied on the change in temperature of a hot wire due to sound-driven air flow around it. A microphone based on a similar idea used an acoustic resonator to detect sound in a narrow frequency band ([Tucker and Paris, 1921](#)). More recently, the Microflown (Microflown Technologies, Arnhem, Netherlands) senses sound across the audible frequency range by also detecting the effect of acoustic flow on the temperature of a thin wire ([de Bree, 2003](#)). This has been a very successful instrument for examining noise sources. In addition, there has been extensive work on sensing fluid flow using beam-like structures that operate similarly to sensory hairs or cilia found on countless small animals ([Asadnia et al., 2016](#); [Bezares-Calderón et al., 2020](#); [Miles, 2019](#); [Tao and Yu, 2012](#)). Sensing acoustic particle velocity could be viewed as an extreme case of sensing fluid flow because the low flow velocities and range of frequencies of interest, spanning several decades, pose enormous challenges. Many of these sensors are designed to resemble the hairs of insects ([Dijkstra et al., 2005](#); [Krijnen et al., 2006](#); [Van Baar et al., 2005](#)). In addition to hairs, we have previously shown that fine fibers, such as spider silk, can respond to airborne sound very accurately over a frequency range from about 1 Hz to 50 kHz ([Miles and Zhou, 2018](#); [Zhou et al., 2022](#); [Zhou and Miles, 2017](#)).

Considering the vast number of species that hear using thin, viscous-driven structures and the myriad designs nature has employed, it is likely that effective engineered designs might also take many forms. For example, if individual hairs or fibers can be effective at sensing sound, it is reasonable to suspect that a two-dimensional structure, such as an array of fibers or a grid or mesh, might also be beneficial ([Zhou et al., 2018](#)). This raises the question of how far apart they should be to ensure maximum viscous drag. If they are too closely spaced, the fluid will not be able to flow through as it acts more like a conventional solid pressure sensor. This question was addressed carefully by [Zalalutdinov et al. \(2017\)](#), who showed that the open spacing between the solid sensing elements should be large enough relative to the thickness of the viscous boundary layer. Many questions remain on how to design an effective acoustic sensor designed to be driven by viscous forces.

It is fairly well-understood that to create a structure that is driven by viscous flow in a sound field, it must have very small dimensions and be lightweight. Because we typically seek to detect sound over a very wide range of sound levels, it is essential to understand how the design parameters impact the sensor's ability to detect the quietest sounds.

This has been quantified various ways for conventional pressure-sensing microphones and described as minimum detectable pressure (MDP; [Zalalutdinov et al., 2017](#)) or equivalently as “pressure-referred noise” ([Miles, 2020](#)). The sensitivity of these acoustic velocity sensors to thermal noise in the medium needs to be well-understood to create effective designs.

The main purpose of this study is to examine the responses to thermal noise and sound of a relatively simple structure that could be used as the sensing element in a flow-sensing microphone: a simple cantilever beam. Knowing the response to thermal noise and the response to sound enables the calculation of the signal to thermal noise ratio. To respond to sound, the beam should have as little mass and stiffness as possible ([Miles, 2020](#)). The beam examined here is motivated by our earlier study of the acoustic response of spider silk, which is driven by sound due to viscous forces in the air ([Miles and Zhou, 2018](#); [Zhou et al., 2022](#); [Zhou and Miles, 2017](#)). The beam is taken to have a rectangular cross section, which is compatible with the constraints of silicon microfabrication. The thickness of each beam is approximately 340 nm. The widths and lengths of the beams were varied to examine the effects of overall beam size on the acoustic response and thermal noise.

To gain confidence in the measured results, comparisons are presented of results obtained from analytical predictions of the responses to sound and thermal noise. The approximate governing differential equations for the beams are easily obtained using classical methods. The interaction of each beam with the surrounding fluid is more difficult to model; it is accounted for by calculating the viscous flow field around the beam ([Miles, 2020](#)).

The response to thermal noise is calculated assuming that the random thermal noise excitation is weakly stationary, fully uncorrelated in space, and time and uniformly distributed along the beam's length. This approximate model leads to a calculation of the power spectral density of the random response at any location along the beam. The damping of the resonant modes is calculated based on the viscous flow around the beam ([Miles, 2020](#)). The response to sound is determined by, again, calculating the force applied to the beam by the moving viscous fluid.

Measured results of the responses to thermal noise excitation and sound were obtained using a laser vibrometer in our anechoic chamber. Because the beam is fabricated using silicon microfabrication methods, it is produced as part of a silicon chip, which can have a significant influence on the viscous acoustic flow around the beam. The influence of the silicon chip on the acoustic flow is accounted for using a finite element model for the flow of the viscous fluid.

The measured and predicted results are shown to be in excellent agreement, suggesting that measurement challenges have not biased the results. The agreement between predictions and measurements also suggests that our approximate assumptions of considering the noise excitation to be fully uncorrelated and weakly stationary along with the approximations of our viscous fluid model do not lead to

noticeable errors, at least for the structures and sound fields examined here.

Because of the well-known importance of the size of pressure-sensing microphone diaphragms on their thermal noise response, here, microbeams are examined having various widths of 2, 3, and 5  $\mu\text{m}$ . In addition, the lengths of the beams were varied from 171 to 500  $\mu\text{m}$ . It is found that for the beams examined here, the surface area, or overall size of the beams, does not have a strong effect on the pressure-referred noise.

Having the power spectral density of the response to thermal noise and the response to sound reveals how the viscous damping of the beam's resonant modes influences the sound pressure-referred noise. These data make it clear that the beam should respond with as few resonant modes as feasible such that the contribution to the power spectral density of the thermal noise response will be minimized.

When the beam is driven by sound through viscous forces due to the relative velocity between the beam and fluid, it is desirable to have as *much* viscous damping as possible so that the beam's motion more closely represents the mean acoustic flow. An increase in the viscous damping, which couples the structure to the fluid, will also reduce the thermal noise response power spectral density. An increase in viscous damping will then lead to an improvement in the signal to thermal noise ratio when the structure is driven using viscous forces. This is the *opposite* of the well-known result in pressure-sensing microphones, where minimizing all sources of damping is essential for minimizing the response to thermal noise (Gabrielson, 1993; Miles, 2020).

It should be noted that damping that occurs as a result of the relative motion of the beam and a fixed boundary does not contribute to the coupling of the beam with the moving fluid and, hence, should be avoided.

To explore further how the viscous damping due to the relative motion of the beam and sound-driven fluid influences the pressure-referred noise, a hypothetical study is conducted in which simulated pressure-referred noise is calculated using an increased value of the viscous damping coefficient for the beam. Of course, in practice, achieving a significant increase in viscous damping would require a significant modification to the beam structure; these calculated results using artificially increased damping are simply to illustrate the performance that might be achieved through designs that increase the viscous damping. In the comparisons presented here, we have left the structural dimensions and material properties unchanged to focus attention only on the influence of the viscous damping on the performance.

The calculated hypothetical results clearly show that the pressure-referred noise is inversely proportional to the effective viscous damping coefficient. This result can also be observed in the equation for the pressure-referred noise. While the results of a mathematical prediction of the pressure-referred noise decrease in proportion to the damping coefficient, the damping also influences other terms in the equations, such as the frequency responses of each resonant mode, making the overall dependence on damping

somewhat obscured. The numerical results plainly show that for the beams examined here, the sound pressure-referred thermal noise is essentially *inversely* proportional to the amount of viscous damping.

In the following, an analytical model for the thermal response of a beam is presented along with a model for the response to sound of a thin beam that is driven by viscous forces in the moving fluid. Experimental results are then presented and compared to those of the analytical model for beams of various widths and lengths. The results show that the pressure-referred noise response of the beams is not significantly affected by changes in the beams' lengths and widths.

## II. ANALYTICAL MODEL FOR THE THERMAL-MECHANICAL RESPONSE OF A BEAM

The thermal noise of microscale cantilever beams has been studied extensively, primarily, because the noise of these beams impacts their use in atomic force microscopy (Butt and Jaschke, 1995). As a primary aim of the present study is to explore the effects of thermal-mechanical noise on the performance of thin beams as acoustic velocity sensors, we will attempt to write down a reasonably detailed model such that the mathematical basis or assumptions for any conclusions is evident.

To avoid distracting details of a complicated sensing structure, in this study, we will limit our attention to a linear, isotropic, and elastic cantilever beam which experiences pure bending due to external forces. The beam is assumed to be surrounded by air that exerts viscous forces as a result of the relative motion between the fluid and beam. The deflection of the beam,  $w(x,t)$ , may be determined by solving a partial differential equation having the form

$$\mathcal{L}(w) + m\ddot{w} + C\dot{w} = f(x,t), \tag{1}$$

where  $\mathcal{L}$  is a linear differential operator,  $m$  is the mass per unit length, and  $C$  is a constant per unit length such that  $C\dot{w}$  gives a restoring force per unit length that is proportional to velocity. In general, we could allow  $\mathcal{L}$ ,  $m$ , and  $C$  to depend on the independent variable,  $x$ .  $f(x,t)$  is the applied force/unit length. If we assume that the structure is a beam having uniform properties along its length, Eq. (1) takes the form of the Euler-Bernoulli beam equation,

$$EIw_{xxxx} + \rho bh\ddot{w} + C\dot{w} = f(x,t), \tag{2}$$

where  $E$  is Young's modulus,  $I$  is the area moment of inertia,  $\rho$  is the mass density,  $b$  is the width,  $h$  is the thickness, and  $m = \rho bh$  is the mass per unit length. The subscripts,  $x$ , denote partial differentiation with respect to  $x$ .  $C$  is the damping constant per unit length.

The value of  $C$  depends on the geometry of the beam and the properties of the fluid flow around the beam that result from its motion. For beams with sufficiently small cross-sectional dimensions and small Reynolds numbers, the flow field can be assumed to be strongly influenced by

viscous effects. The calculation of the viscous damping of beams has been studied extensively by Sader and others to understand the effects of fluid damping on the dynamic response of beams used in atomic force microscope probes (Chon *et al.*, 2000; Sader, 1998). The viscous damping of the beam plays a critical role in determining its response to acoustic particle velocity.

There have been a number of studies of the fluid forces on the vibration of thin beams. Bhiladvala and Wang (2004) studied the influence of fluid damping on the quality factor ( $Q$ ) and damped resonance frequency of micron and submicron scale beams oscillating at MHz frequencies. In this high ultrasonic frequency range, it is shown that a continuum model of the gas is not appropriate for submicron scale beams. Because our primary interest here is on the audible frequency range, we have employed a continuum model following the approach described by Stokes (1851). Blom *et al.*, (1992) explained the relationship between the natural frequencies of the beams and the atmospheric pressure and also concluded that the critical atmospheric pressure to obtain a large quality factor is almost independent of the beam length but decreases strongly with increasing width and thickness of the beams, which are intended to be used as resonators. Similarly, it was shown by Verbridge *et al.* (2008) that smaller resonators had higher quality factors ( $Q$ ) under ambient conditions, although the question on the frequency-dependence of  $Q$  in vacuum is left open. A study by Jandak *et al.* (2016) showed that the quality factor of micromachined beams depended on the boundary conditions of clamped-clamped and clamped-free cases that were considered in their work. Effect of air pressure on the damping of microcantilever beams was measured by Sumali and Carne (2007), who found that the damping force has a nearly linear relationship with pressure. Through discovery of the gas force per unit length, Bidkar *et al.* (2009) calculated the damping ratio for several modes of a single resonator, which ranged from tens to hundreds of microns in width, in free space and low ambient pressures. They proposed a semi-analytical closed-form model for long microcantilevers which deviates from experimental results at a certain pressure range.

In the model used here to estimate the value of the beam's damping constant,  $C$ , the beam is assumed to be infinitesimally thin and the flow velocity is normal to the beam's surface at distances very far from the beam as described in Miles (2020). The viscous force on the beam is determined by solving the Navier-Stokes equations in which viscous effects dominate, i.e., at small Reynolds numbers.

It can be convenient to express the displacement as a sum of the eigenfunctions,  $\phi_i(x)$ , corresponding to either Eq. (1) or (2), such that

$$w(x, t) = \sum_{i=1}^{\infty} \eta_i(t) \phi_i(x), \quad (3)$$

where  $\eta_i(t)$  are unknowns. The orthogonality of the eigenfunctions facilitates determination of  $\eta_i(t)$ , which may be shown to satisfy

$$\ddot{\eta}_i(t) + \omega_i^2 \eta_i(t) + 2\omega_i \zeta_i \dot{\eta}_i(t) = q_i(t), \quad (4)$$

where  $\omega_i$  is the natural frequency,  $\zeta_i$  is the damping ratio for mode  $i$ , and  $q_i(t)$  is the effective "modal" force for mode  $i$ . Equation (4) enables us to express the solution of Eq. (2) in the form

$$w(x, t) = \int_0^t \int_0^l G(x, r, t, \tau) f(r, \tau) dr d\tau, \quad (5)$$

where

$$G(x, r, t, \tau) = G(x, r, t - \tau) = \sum_{j=1}^{\infty} \frac{\phi_j(x) \phi_j(r) h_j(t - \tau)}{\int_0^l \rho b h \phi_j^2(y) dy} \quad (6)$$

is the Green's function for the beam, and  $h_j$  is the impulse response for mode  $j$ .

Because the excitation,  $f(x, t)$ , is a random function of the independent variables,  $x$  and  $t$ , we seek appropriate statistics to examine the response. Having the solution for the response expressed as Eq. (5) enables us to write the cross correlation of the response at two locations,  $x_1$  and  $x_2$ , and at two times,  $t_1$  and  $t_2$ , as

$$\begin{aligned} E[w(x_1, t_1)w(x_2, t_2)] &= R_{ww}(x_1, x_2, t_1, t_2) \\ &= \int_0^{t_1} \int_0^{t_2} \int_0^l \int_0^l G(x_1, r_1, t_1 - \tau_1) \\ &\quad \times G(x_2, r_2, t_2 - \tau_2) \\ &\quad \times E[f(r_1, \tau_1)f(r_2, \tau_2)] dr_2 dr_1 d\tau_1 d\tau_2, \end{aligned} \quad (7)$$

where  $E[\cdot \cdot \cdot]$  denotes the expected value. The random noise excitation may be assumed to be weakly stationary in time such that  $R_{ww}(x_1, x_2, t_1, t_2) = R_{ff}(r_1, r_2, \tau_2 - \tau_1)$ , which is the cross correlation of the forces at  $r_1$  and  $r_2$ . This may be expressed as the inverse Fourier transform of the cross-power spectral density,  $S_{ff}(r_1, r_2, \omega)$ ,

$$\begin{aligned} E[f(r_1, \tau_1)f(r_2, \tau_2)] &= R_{ff}(r_1, r_2, \tau_2 - \tau_1) \\ &= \int_{-\infty}^{\infty} S_{ff}(r_1, r_2, \omega) e^{i\omega(\tau_2 - \tau_1)} d\omega. \end{aligned} \quad (8)$$

Substituting Eq. (8) into Eq. (7) and changing the order of integration gives

$$\begin{aligned} E[w(x_1, t_1)w(x_2, t_2)] &= R_{ww}(x_1, x_2, t_1, t_2) \\ &= \int_{-\infty}^{\infty} \int_0^{t_1} \int_0^{t_2} \int_0^l \int_0^l G(x_1, r_1, t_1 - \tau_1) \\ &\quad \times G(x_2, r_2, t_2 - \tau_2) S_{ff}(r_1, r_2, \omega) \\ &\quad \times e^{i\omega(\tau_2 - \tau_1)} dr_2 dr_1 d\tau_1 d\tau_2 d\omega. \end{aligned} \quad (9)$$

The integrations in the time domain may be modified by the substitutions  $\tau'_1 = t_1 - \tau_1$  and  $\tau'_2 = t_2 - \tau_2$ . Because the impulse responses,  $h_j(\tau)$ , in Eq. (6) are zero for  $\tau < 0$ , we

can replace  $t_1$  and  $t_2$  in the upper limits of integration in Eq. (9) by  $\infty$  without changing the result. We can also replace the lower limits of integration by  $-\infty$  as we are interested in only the steady-state statistics, i.e., as  $t \rightarrow \infty$ .

We can also let

$$\mathcal{G}^*(x_1, r_1, \omega) = \int_{-\infty}^{\infty} G(x_1, r_1, \tau) e^{i\omega\tau} d\tau \quad (10)$$

and

$$\mathcal{G}(x_2, r_2, \omega) = \int_{-\infty}^{\infty} G(x_2, r_2, \tau) e^{-i\omega\tau} d\tau, \quad (11)$$

where the superscript “\*” denotes the complex conjugate, and we have used the fact that  $G(x, r, t - \tau)$ , as defined in Eq. (6), is real.

After some rearranging, Eqs. (9)–(11) lead to an expression having the form of the inverse Fourier transform of the response cross-power spectral density, which leads to

$$S_{ww}(x_1, x_2, \omega) = \int_0^l \int_0^l \mathcal{G}^*(x_1, r_1, \omega) \mathcal{G}(x_2, r_2, \omega) \times S_{ff}(r_1, r_2, \omega) dr_2 dr_1. \quad (12)$$

The frequency response function of mode  $j$ ,  $H_j(\omega)$ , is related to the impulse response  $h_j(\tau)$  by

$$H_j(\omega) = \int_0^{\infty} h_j(\tau) e^{i\omega\tau} d\tau. \quad (13)$$

Again, because the impulse response is zero for negative values of  $\tau$ , Eqs. (6), (11), and (13) yield

$$\mathcal{G}(x, r, \omega) = \sum_{j=1}^{\infty} \frac{\phi_j(x)\phi_j(r)H_j(\omega)}{\int_0^l \rho bh \phi_j^2(y) dy}. \quad (14)$$

### III. RANDOM RESPONSE TO SPATIALLY UNCORRELATED IDEAL WHITE NOISE

To calculate the response of the beam due to thermal excitation, we will determine its response to a spatially random field in which the forces applied at any two spatial locations,  $x_1$  and  $x_2$ , are fully uncorrelated. We will also assume that the forces at any two instants of time,  $t_1$  and  $t_2$ , are also uncorrelated. These approximations lead to a power spectral density which is not dependent on the temporal frequency,  $\omega$ , i.e., white noise. In addition, the wave vector spectrum of the force is not dependent on the spatial frequency,  $k$ . The cross correlation of the force in Eq. (8) becomes

$$R_{ff}(r_1, r_2, \tau_2 - \tau_1) = \delta(r_1 - r_2)\delta(\tau_1 - \tau_2)K, \quad (15)$$

where  $K$  is a constant and  $\delta(\cdot)$  is the Dirac delta function. The Fourier transform of this cross correlation function is the cross-power spectral density.

Because the cross correlation function depends on two independent variables (time and space), the power spectral density is, in general, dependent on a temporal frequency,  $\omega$ , (rad/s) and a spatial frequency,  $k$  (1/m). Note that this spatial frequency is denoted by a lowercase  $k$  while the constant,  $K$ , in Eq. (15) is uppercase. Because the cross correlation functions are given by Dirac delta functions, the power spectral density becomes independent of temporal and spatial frequencies. Again, as the random force is assumed to be weakly stationary in time, Eq. (15) depends only on the difference,  $\tau = \tau_1 - \tau_2$ . We also assume that the random force is homogeneous in space such that it depends only on the difference,  $r_1 - r_2 = \Delta r$ . The two-dimensional Fourier transform of Eq. (15) then gives the two-dimensional power spectral density of the force,

$$\begin{aligned} S_{ff}(\omega, k) &= \frac{1}{(2\pi)^2} \int_{-\infty}^{\infty} \int_{-\infty}^{\infty} e^{-i\Delta r k} e^{-i\omega\tau} R_{ff}(\Delta r, \tau) d\Delta r d\tau \\ &= \frac{1}{(2\pi)^2} \int_{-\infty}^{\infty} \int_{-\infty}^{\infty} e^{-i\Delta r k} e^{-i\omega\tau} \delta(\Delta r)\delta(\tau) \\ &\quad \times K d\Delta r d\tau = \frac{K}{(2\pi)^2}. \end{aligned} \quad (16)$$

The power spectral density of the force is then independent of the temporal and spatial frequencies,  $\omega$  and  $k$ . This is typically referred to as “white noise.” The constant,  $K$ , is

$$K = (2\pi)^2 S_{ff}(\omega, k) = (2\pi)^2 S_{ff}. \quad (17)$$

If the force,  $f(t)$ , in Eq. (3) has the units of N/m, the two-dimensional power spectral density,  $S_{ff}$ , will have the units of

$$(\text{N/m})^2 / (\text{rad/s}) / (1/\text{m}) = (\text{N/m})^2 \text{m s/rad}. \quad (18)$$

In this special case, Eqs. (12) and (14) lead to

$$S_{ww}(x_1, x_2, \omega) = \sum_{j=1}^{\infty} \frac{(2\pi)^2 S_{ff} \phi_j(x_1)\phi_j(x_2) |H_j(\omega)|^2 \int_0^l \phi_j^2(x) dx}{(\rho bh)^2 \left( \int_0^l \phi_j^2(y) dy \right)^2}, \quad (19)$$

where we have used the fact that the eigenfunctions are orthogonal and assumed that  $\rho bh$  is independent of  $x$ . We may let  $x_1 = x_2$  to compute the auto-power spectral density.

The frequency dependence of the power spectral density of the response in Eq. (19) is determined by the modal frequency response functions,  $H_j(\omega)$ . These are of the form

$$H_j(\omega) = \frac{1}{\omega_j^2 - \omega^2 + 2i\omega\omega_j\zeta_j}, \quad (20)$$

where  $\omega_j$  is the  $j$ th natural frequency, and  $\zeta_j$  is the damping ratio of mode  $j$ . The natural frequencies depend only on the system’s stiffness and mass and how these are distributed

along the  $x$  direction. Substitution of each eigenfunction into Eq. (2) leads to a set of ordinary differential equations for the response of each mode. The natural frequencies may be determined by solving Eq. (2) with no force applied and using the appropriate boundary conditions. This also leads to

$$2\omega_j \zeta_j = \frac{C}{\rho b h}. \quad (21)$$

The frequency response functions in Eq. (20) then simplify to

$$H_j(\omega) = \frac{1}{\omega_j^2 - \omega^2 + i \frac{\omega C}{\rho b h}}. \quad (22)$$

#### IV. FORCE DUE TO THERMAL NOISE

We now need to relate the power spectral density of the random force,  $S_{ff}$ , to the properties of the air. To do this, we will use the equipartition theorem, which relates the kinetic and potential energies of each degree of freedom of the system to the kinetic energy of the gas (Kittel, 1958).

The expected value of the beam's total kinetic energy may be expressed as

$$E[T] = \frac{1}{2} \rho b h \int_0^L E[\dot{w}(x, t)^2] dx, \quad (23)$$

where we assume that the density,  $\rho$ , the width,  $b$ , and the thickness,  $h$ , are all independent of  $x$ . We may express the mean square velocity,  $E[\dot{w}(x, t)^2]$ , in terms of the power spectral density of the displacement,  $S_{ww}(x_1, x_2, \omega)$ . Letting  $x_1 = x_2 = x$ ,

$$E[\dot{w}(x, t)^2] = \int_{-\infty}^{\infty} \omega^2 S_{ww}(x, x, \omega) d\omega. \quad (24)$$

Substituting Eq. (24) into Eq. (23) results in

$$E[T] = \frac{1}{2} \rho b h \int_0^L \int_{-\infty}^{\infty} \omega^2 S_{ww}(x, x, \omega) d\omega dx. \quad (25)$$

This total kinetic energy may be expressed as a summation over all of the modes using Eq. (19) such that

$$\begin{aligned} E[T] &= \frac{1}{2} \rho b h \int_0^L \int_{-\infty}^{\infty} \omega^2 \sum_{j=1}^{\infty} \frac{(2\pi)^2 S_{ff} \phi_j^2(x) |H_j(\omega)|^2 \int_0^L \phi_j^2(y) dy}{(\rho b h)^2 \left( \int_0^L \phi_j^2(y) dy \right)^2} d\omega dx \\ &= \sum_{j=1}^{\infty} \frac{1}{2} \int_0^L \int_{-\infty}^{\infty} \omega^2 \frac{(2\pi)^2 S_{ff} \phi_j^2(x) |H_j(\omega)|^2 \int_0^L \phi_j^2(y) dy}{\rho b h \left( \int_0^L \phi_j^2(y) dy \right)^2} d\omega dx = \sum_{j=1}^{\infty} E[T_j]. \end{aligned} \quad (26)$$

The kinetic energy of mode  $j$  is then

$$E[T_j] = \frac{1}{2} \int_0^L \int_{-\infty}^{\infty} \omega^2 \frac{(2\pi)^2 S_{ff} \phi_j^2(x) |H_j(\omega)|^2 \int_0^L \phi_j^2(x) dx}{\rho b h \left( \int_0^L \phi_j^2(y) dy \right)^2} d\omega dx. \quad (27)$$

The integration over  $\omega$  may be performed using contour integration (Miles, 2020) after substituting Eq. (20) for  $H_j(\omega)$  and using Eq. (21) to obtain

$$\int_{-\infty}^{\infty} \omega^2 |H_j(\omega)|^2 d\omega = \frac{\pi}{2\omega_j \zeta_j} = \frac{\pi \rho b h}{C}. \quad (28)$$

Equation (27) may then be simplified to

$$\begin{aligned} E[T_i] &= \frac{1}{2} \frac{\pi}{C} \int_0^L \frac{(2\pi)^2 S_{ff} \phi_j^2(x) \int_0^L \phi_j^2(y) dy}{\left( \int_0^L \phi_j^2(y) dy \right)^2} dx \\ &= \frac{1}{2} \frac{\pi (2\pi)^2 S_{ff}}{C}. \end{aligned} \quad (29)$$

Note that the expected value of the kinetic energy for mode  $i$  is independent of mode number. That is, it is the same for all modes. We can then say that the energy is equally distributed or "partitioned" between all of the degrees of freedom of the structure (Kittel, 1958). This is a consequence of our assumption that the force consists of a spatially and temporally uncorrelated random field as in Eq. (15).

Because we are interested in the random response due to thermal noise, we need to express this power spectral density of the force in terms of the temperature of the surrounding gas. If the random response of the beam is weakly

stationary (that is, the first order statistics are not varying with time), the expected value of the kinetic energy of each degree of freedom will equal the expected value of the potential energy of each degree of freedom. The equipartition theorem tells us that these mean degree of freedom energies will equal the kinetic energy of the gas, which may be calculated knowing the absolute temperature,  $T$ , and Boltzmann's constant,  $K_B$ , such that

$$\frac{1}{2}K_B T = E[V_i] = E[T_i], \tag{30}$$

where  $E[V_i]$  is the expected value of the randomly fluctuating potential energy of degree of freedom (or resonant mode),  $i$ , of the beam, and  $E[T_i]$  is the expected value of the randomly fluctuating kinetic energy of the  $i$ th mode. These expected values may be computed from our expressions above for the power spectral density of the beam's response.

Equations (30) and (29) enable us to express the power spectral density of the random thermal excitation in terms of the temperature,

$$\frac{1}{2}K_B T = \frac{1}{2} \frac{\pi(2\pi)^2 S_{ff}}{C} \tag{31}$$

or

$$S_{ff} = \frac{K_B T C}{\pi(2\pi)^2}. \tag{32}$$

The force that results from thermal noise is, thus, strongly dependent on the energy dissipation, which, in this case, is proportional to the dashpot constant,  $C$  (Gabrielson, 1993). The equipartition theorem has led us to an expression for the power spectral density of the force,  $f(x,t)$ , in Eq. (2) that depends only on the damping coefficient,  $C$ , in Eq. (2), the temperature,  $T$ , and Boltzmann's constant,  $K_B$ . Note that this result does not depend on any properties of the beam or its resonant modes or degrees of freedom.

Equation (32) may be used in Eq. (19) to compute the power spectral density of the response at the location  $x$  due to thermal noise,

$$S_{ww}(x, x, \omega) = \sum_{j=1}^{\infty} \frac{K_B T C \phi_j^2(x) |H_j(\omega)|^2}{\pi(\rho b h)^2 \int_0^l \phi_j^2(y) dy}. \tag{33}$$

If the damping constant,  $C$ , is not too large, this spectral density will have maxima at each resonant frequency,  $\omega_j$ . If the response at  $\omega \approx \omega_j$  is dominated by the contribution from only mode  $j$ , then evaluating Eq. (33) at  $\omega = \omega_j$  gives

$$S_{ww}(x, x, \omega_j) \approx \frac{K_B T \phi_j^2(x)}{\pi \omega_j^2 C \int_0^l \phi_j^2(y) dy}. \tag{34}$$

The power spectral density of the velocity at each resonance simply becomes

$$S_{\dot{w}\dot{w}}(x, x, \omega_j) \approx \frac{K_B T \phi_j^2(x)}{\pi C \int_0^l \phi_j^2(y) dy}. \tag{35}$$

Increasing the damping constant,  $C$ , will clearly reduce the beam's response to thermal noise excitation at the frequency  $\omega_j$ .

Note that having the power spectral density of the force in Eq. (32) also allows us to calculate the power spectral density of the response,  $S_{ww}(x, x, \omega)$ , by other methods that do not require knowledge of the uncoupled resonant modes. There are structures, for example, having nonproportional damping, where the solution for the uncoupled eigenfunctions is cumbersome compared to a more direct solution approach (Miles, 2020).

## V. RESPONSE DUE TO ACOUSTIC FLOW

Having a means of calculating the response of beams to thermal noise excitation, our task now is to determine the response of the beams to sound when their dimensions are sufficiently small such that viscous forces in the air dominate. These beams are quite thin and narrow, having thicknesses significantly less than  $1 \mu\text{m}$  and widths on the order of a few microns. These will typically be made using silicon microfabrication, where the material has been deposited using a process in which the material properties of the structure can be quite difficult to control and/or characterize. Our main interest here is more on the interaction of the fluid with the beams than on the material properties that determine the beam stiffness and mass, i.e., the density,  $\rho$ , and the Young's modulus,  $E$ . For our purposes, these stiffness and mass properties are determined empirically.

The sound field is taken to be a single ideal plane wave propagating in the positive  $x$  direction in which the fluctuating pressure and fluctuating acoustic particle velocity are related to each other by the constant acoustic impedance,  $\rho_0 c$ , where  $\rho_0$  is the air density and  $c$  is the speed of propagation of acoustic waves (Miles, 2020). As is common, we will characterize the amplitude of the sound wave in terms of the sound pressure in pascals. Because the dimensions of the beam are very small relative to the acoustic wavelength at the frequencies of interest, the force on the structure is mainly the result of the viscosity of the fluid rather than the sound pressure, which dominates when the structure is sufficiently large. The viscous acoustic force is assumed to be proportional to the relative velocity of the fluid,  $\dot{y}$ , and beam,  $\dot{w}(x, t)$ . If the beam's cross section does not vary with position,  $x$ , along the length, then we can assume that the viscous force is simply proportional to the relative velocity, where the constant of proportionality is the viscous damping coefficient,  $C$ . Again,  $C\dot{w}(x, t)$  will be the viscous damping force per unit length.

Let  $\mathcal{W}$  denote the deflection of the beam due to viscous flow. The force per unit length resulting from the excitation in Eqs. (1) and (2) then becomes

$$f(x, t) = \mathcal{F}(t) = C\dot{y}, \tag{36}$$

where, again, the flow velocity,  $\dot{y}$ , is assumed to be independent of the spatial position,  $x$ . Equations (2) and (36) enable us to express the governing equation of the beam as

$$EIw_{xxxx} + \rho b h \ddot{w} = C(\dot{y} - \dot{w}). \tag{37}$$

The net viscous force on the right hand side of Eq. (37) is clearly proportional to the relative velocity between the beam and fluid,  $\dot{y} - \dot{w}$ . Because we have assumed that the flow velocity,  $\dot{y}$ , does not depend on the spatial position,  $x$ , the cross-power spectral density of the force applied by the fluid motion,  $\dot{y}$ , becomes equal to the auto-power spectral density and is independent of the spatial coordinate,

$$S_{\mathcal{F}\mathcal{F}}(r_1, r_2, \omega) = S_{\mathcal{F}\mathcal{F}}(\omega) = C^2 S_{\dot{y}\dot{y}}(\omega) = C^2 S_{pp}(\omega) / (\rho_0 c)^2. \tag{38}$$

Consequently, the integrations over  $r_1$  and  $r_2$  as in Eq. (9) become separated such that

$$\begin{aligned} R_{\mathcal{W}\mathcal{W}}(x_1, x_2, t_1, t_2) &= \int_{-\infty}^{\infty} \int_0^{t_1} \int_0^{t_2} \int_0^l \int_0^l G(x_1, r_1, t_1 - \tau_1) \\ &\quad \times G(x_2, r_2, t_2 - \tau_2) S_{\mathcal{F}\mathcal{F}}(\omega) \\ &\quad \times e^{i\omega(\tau_2 - \tau_1)} dr_2 dr_1 d\tau_1 d\tau_2 d\omega \\ &= \int_{-\infty}^{\infty} \int_0^{t_1} \int_0^{t_2} \left[ \int_0^l G(x_1, r_1, t_1 - \tau_1) dr_1 \right] \\ &\quad \times \left[ \int_0^l G(x_2, r_2, t_2 - \tau_2) dr_2 \right] \\ &\quad \times e^{i\omega(\tau_2 - \tau_1)} d\tau_1 d\tau_2 S_{\mathcal{F}\mathcal{F}}(\omega) d\omega. \end{aligned} \tag{39}$$

We can, again, recognize this to be the inverse Fourier transform of the cross-power spectral density, which is then

$$S_{\mathcal{W}\mathcal{W}}(x_1, x_2, \omega) = S_{\mathcal{F}\mathcal{F}}(\omega) \left[ \int_0^l \mathcal{G}^*(x_1, r_1, \omega) dr_1 \right] \times \left[ \int_0^l \mathcal{G}(x_2, r_2, \omega) dr_2 \right]. \tag{40}$$

Using Eq. (14), the integrations may be written as

$$\int_0^l \mathcal{G}(x, r, \omega) dr = \sum_{j=1}^{\infty} \frac{\phi_j(x) H_j(\omega)}{\int_0^l m \phi_j^2(y) dy} \int_0^l \phi_j(r) dr. \tag{41}$$

Equations (40) and (41) show that in the case of this acoustic flow excitation, the eigenfunctions that have small average values over the length do not contribute significantly to the response because they tend to be orthogonal to the force, which, again, we have taken to be independent of spatial position,  $x$ . This differs from the result that we obtained for spatially random noise in Eq. (33), where all modes contribute equally. Equations (40) and (41) may be used to calculate the power spectral density of the deflection,  $S_{\mathcal{W}\mathcal{W}}(x, x, \omega)$ , relative to the power spectral density of the acoustic pressure,  $S_{pp}(\omega)$ , at one location,  $x$ ,

$$\begin{aligned} \frac{S_{\mathcal{W}\mathcal{W}}(x, x, \omega)}{S_{pp}(\omega)} &= \frac{C^2}{(\rho_0 c)^2} \left[ \sum_{j=1}^{\infty} \frac{\phi_j(x) H_j^*(\omega)}{\int_0^l m \phi_j^2(y) dy} \int_0^l \phi_j(r) dr \right] \\ &\quad \times \left[ \sum_{i=1}^{\infty} \frac{\phi_i(x) H_i(\omega)}{\int_0^l m \phi_i^2(y) dy} \int_0^l \phi_i(r) dr \right]. \end{aligned} \tag{42}$$

Having expressions for the power spectral density of the response to sound (the signal) in Eq. (42) and that due to thermal noise in Eq. (33), we can obtain the pressure-referred noise. This would next give a measure of how much sound pressure would elicit the amount of signal that we obtain as a result of noise. This pressure-referred noise is then

$$S_{pp\text{thermal}}(\omega) = \frac{S_{\mathcal{W}\mathcal{W}}(\omega)}{S_{\mathcal{W}\mathcal{W}}(x, x, \omega) / S_{pp}(\omega)} = \frac{K_B T C \sum_{j=1}^{\infty} \phi_j^2(x) |H_j(\omega)|^2}{\pi (\rho b h)^2 \int_0^l \phi_j^2(y) dy} \frac{C^2}{(\rho_0 c)^2} \frac{\left[ \sum_{j=1}^{\infty} \frac{\phi_j(x) H_j^*(\omega)}{\int_0^l m \phi_j^2(y) dy} \int_0^l \phi_j(r) dr \right] \left[ \sum_{i=1}^{\infty} \frac{\phi_i(x) H_i(\omega)}{\int_0^l m \phi_i^2(y) dy} \int_0^l \phi_i(r) dr \right]}{\left[ \sum_{j=1}^{\infty} \frac{\phi_j(x) H_j^*(\omega)}{\int_0^l m \phi_j^2(y) dy} \int_0^l \phi_j(r) dr \right] \left[ \sum_{i=1}^{\infty} \frac{\phi_i(x) H_i(\omega)}{\int_0^l m \phi_i^2(y) dy} \int_0^l \phi_i(r) dr \right]}. \tag{43}$$

This can be simplified somewhat, and using the fact that  $m = \rho b h$ ,

$$S_{pp\text{thermal}}(\omega) = \frac{K_B T (\rho_0 c)^2}{C \pi} \frac{\sum_{j=1}^{\infty} \frac{\phi_j^2(x) |H_j(\omega)|^2}{\int_0^l \phi_j^2(y) dy}}{\left[ \sum_{j=1}^{\infty} \frac{\phi_j(x) H_j^*(\omega)}{\int_0^l \phi_j^2(y) dy} \int_0^l \phi_j(r) dr \right] \left[ \sum_{i=1}^{\infty} \frac{\phi_i(x) H_i(\omega)}{\int_0^l \phi_i^2(y) dy} \int_0^l \phi_i(r) dr \right]}. \tag{44}$$



As in Eq. (33), if the damping constant,  $C$ , is not too large, resonant peaks will dominate the responses to sound and thermal excitation. In this case, we may assume that each summation in Eq. (44) is dominated by a single term when  $\omega \approx \omega_j$ . Equation (44) may then be approximated by

$$S_{pp\text{thermal}}(\omega_j) \approx \frac{K_B T (\rho_0 c)^2 \int_0^l \phi_j^2(y) dy}{C \pi \left[ \int_0^l \phi_j(r) dr \right]^2}. \tag{45}$$

Again, this shows that the viscous damping constant,  $C$ , is a key parameter in determining the pressure-referred noise. Increasing  $C$  will reduce the influence of thermal noise.

We should examine the units of Eq. (44). The power spectral density,  $S_{pp\text{thermal}}$ , should have units of  $\text{Pa}^2/(\text{rad/s})$ . First, note that if the eigenfunctions,  $\phi_j$ , are expressed with units, the units will cancel because  $\phi_j$  always appears with equal exponents in the numerator and denominator in each term. The complex frequency response functions,  $H_j(\omega)$ , also appear squared in numerator and denominator, so their units also cancel. The only remaining term contributing units in the complicated fraction,

$$\frac{\sum_{j=1}^{\infty} \frac{\phi_j^2(x) |H_j(\omega)|^2}{\int_0^l \phi_j^2(y) dy}}{\left[ \frac{\sum_{j=1}^{\infty} \frac{\phi_j(x) H_j^*(\omega)}{\int_0^l \phi_j^2(y) dy} \int_0^l \phi_j(r) dr \right] \left[ \frac{\sum_{i=1}^{\infty} \frac{\phi_i(x) H_i(\omega)}{\int_0^l \phi_i^2(y) dy} \int_0^l \phi_i(r) dr \right]}, \tag{46}$$

will then be the differential length  $dr$  or  $dy$  in the denominator. The units of the fraction in Eq. (46) will then be  $1/\text{length}$ , i.e.,  $1/\text{m}$ .

Boltzmann’s constant,  $K_B$ , is normally expressed with units of J per deg K such that  $K_B T$  has the units of J or  $\text{N} \times \text{M}$ . The units of the acoustic impedance,  $\rho_0 c$ , will be  $\text{P} \times \text{s}/\text{m}$ , or  $\text{N}/\text{m}^2 \times \text{s}/\text{m}$ . As mentioned above after Eq. (2),  $C\dot{w}$  will be the damping force per unit length so the units of the dashpot constant,  $C$ , will be  $\text{N} \times \text{s}/\text{m}^2$ . Combining the units of the first fraction on the right hand side of Eq. (44) then gives

$$\frac{K_B T (\rho_0 c)^2}{C \pi} \rightarrow \frac{(\text{N} \times \text{m}) \times (\text{N}/\text{m}^2 \times \text{s}/\text{m})^2}{\text{N} \times \text{s}/\text{m}^2} = \frac{\text{N}^2 \times \text{s}}{\text{m}^3}. \tag{47}$$

The product on the right hand side of Eq. (44) will then have the units of

$$\frac{\text{N}^2 \times \text{s}}{\text{m}^3} \times \frac{1}{\text{m}} = \frac{\text{N}^2 \times \text{s}}{\text{m}^4} = \frac{\text{P}^2}{\text{rad/s}}, \tag{48}$$

which are the correct units of the power spectral density,  $S_{pp\text{thermal}}$ .

One aim of this study is to examine how the pressure-referred noise of the viscous-driven beam depends on the viscous damping coefficient,  $C$ . The result of Eq. (44) is clearly inversely proportional to  $C$  such that we can conclude that increasing  $C$  should decrease the pressure-referred noise.

The determination of the dashpot constant,  $C$ , can be a bit difficult and depends on the geometry of the structure being examined. The approach used to obtain the relation between the pressure on the beams because of their motion relative to the surrounding viscous fluid is described in Sec. 9.8 of Miles (2020). The calculations assume that the air density is  $\rho = 1.2064 \text{ kg}/\text{m}^3$ , the sound speed is  $c = 344 \text{ m}/\text{s}$ , and the dynamic viscosity of air is  $\mu = 1.8075 \times 10^{-5} \text{ kg}/(\text{m s})$ .

Note also that the frequency response functions,  $H$ , that appear in Eq. (44) also depend on  $C$ , as shown in Eq. (22). This can make it somewhat difficult to see the overall sensitivity of the pressure-referred thermal noise to changes in the damping constant,  $C$ , because the complex frequency response functions are summed in the numerator and denominator in Eq. (44). Whereas the exact dependence on  $C$  in Eq. (44) depends on frequency,  $\omega$ , the natural frequencies,  $\omega_j$ , and the eigenfunctions,  $\phi_j(x)$ , we can expect the effects of  $C$  on the numerator and denominator to tend to cancel each other, leaving its net impact to be determined mainly by the factor of  $C$  in the denominator of the leading term. Rather than presenting a general expression for the dependence of the pressure-referred noise on  $C$ , it may be more instructive to examine numerical results for the beam geometries considered here. The results presented in the following show that  $S_{pp\text{thermal}}$  remains inversely proportional to the viscous damping constant,  $C$ , for beams such as these.

## VI. COMPARISON WITH EXPERIMENTS

Measurements have been performed for silicon cantilever beams having several widths and lengths to obtain the responses resulting from thermal noise and acoustic excitation. The experiments are conducted in the anechoic chamber at Binghamton University. The chamber interior dimensions are 4.2 m wide, 5.4 m long, and 3.2 m tall. The absorbent wedges that cover all surfaces are made of fiberglass. The chamber has been certified by the manufacturer to provide an anechoic environment at all frequencies above 80 Hz. The noise floor of the chamber is approximately 0 dBA. The anechoic chamber was tested using methods specified in ISO 3745 (2003).

The beams are fabricated on a silicon chip over a central square through-hole. The dimensions of the chip are  $2 \text{ mm} \times 2 \text{ mm} \times 0.5 \text{ mm}$ . The central through-hole is  $505 \mu\text{m} \times 505 \mu\text{m} \times 505 \mu\text{m}$ . The beams are  $500 \mu\text{m}$  long, and each is composed of three layers of film having equal thickness, a layer of poly-crystalline silicon having a thickness of  $h_{\text{poly}} \approx 0.113 \mu\text{m}$ , surrounded by silicon nitride layers each having the same thickness of  $h_{\text{nitride}} \approx 0.113 \mu\text{m}$ .

for a total beam thickness of approximately  $h \approx 0.34 \mu\text{m}$ . Measurements were performed on beams having widths of  $B = 2, 3, \text{ and } 5 \mu\text{m}$ . The widths of these beams are sufficiently small relative to the wavelength of sound in the audible frequency range such that the dominant acoustic excitation is very likely to be the result of the viscosity of air.

In the calculations here, we have assumed that the composite beams have an equivalent isotropic density of

$$\rho_{\text{beam}} \approx 2600 \text{ kg/m}^3. \quad (49)$$

The equivalent Young's modulus of the composite beams is taken to be

$$E \approx 1.48 \times 10^{11} \text{ N/m}^2. \quad (50)$$

The beams are fabricated over a hole in the silicon chip as depicted in Fig. 1.

The motion of each beam is measured using a laser doppler vibrometer (Polytec OFV-534, Polytech GmbH, Waldbronn, Germany). The laser is placed at a distance to avoid acoustic reflection for the acoustic response measurement and close to the test object with a  $100\times$  close-up lens for maximum signal to noise ratio for the thermal noise measurement. For acoustic stimulation, step sinusoidal signals and time-domain windowing are used to acquire the acoustical frequency response while eliminating the acoustical reflection and uncorrelated noise (Lai *et al.*, 2022). Measurements were performed at normal atmospheric pressure and temperature. The reference microphone (B&K type 4138 1/8 in.) is placed adjacent to the chip. Measurements obtained at an array of locations around the test sample show that the sound field closely approximates that of an ideal plane acoustic wave. The well-known relation between sound pressure and acoustic particle velocity in a one-dimensional plane wave can then be used to relate the measured sound pressure to the acoustic particle velocity near

the test object. National Instruments PXI 1033 data acquisition system (National Instruments, Austin, TX) is used for data acquisition. The laser is focused on the tip of the beam as displayed in Fig. 2.

The noise root power spectral density is calculated from the measured beam velocity resulting from thermal noise excitation. The measured results for all three beam widths are compared to predictions obtained using Eq. (44) in Fig. 3. The results show excellent agreement between measurements and predictions, which suggests that the measurement method and assumptions of the predictions are not overly biased by errors.

The acoustical frequency response of the beams is measured in the anechoic chamber using stepped sinusoidal pure tones and narrow band least squares curve fitting (Lai *et al.*, 2022). This process can greatly reduce the influence of any acoustic reflection and any uncorrelated acoustic noise from the equipment or electromagnetic noise.

In examining the response of the beams to acoustic flow, it is important to be able to measure the motion of the beams and the velocity of the sound-induced flow around the beams. Of course, measuring the motion of the air can be quite difficult. The sound-induced air velocity can be significantly affected by the boundary conditions imposed by the structure used to support the silicon beams. This structure includes the silicon chip itself and any structure used to hold the chip. To estimate the acoustic flow near the beams displayed in Fig. 1, a COMSOL (COMSOL, Inc., Burlington, MA) finite element model was constructed. This model estimates the acoustic flow around the chip and through the hole in which the beams reside and is shown in Fig. 1. This model was used to estimate  $V_{\text{air}}$ , employed to normalize the measured velocity of the tips of the beams in Fig. 4. Because the hole containing the beams takes up only a fraction of the planar surface of the chip, the air velocity within the hole can be greater than that far from the chip,  $V_{\text{air}}$ . This can cause the velocity of the tip of each beam to be greater than  $V_{\text{air}}$ .

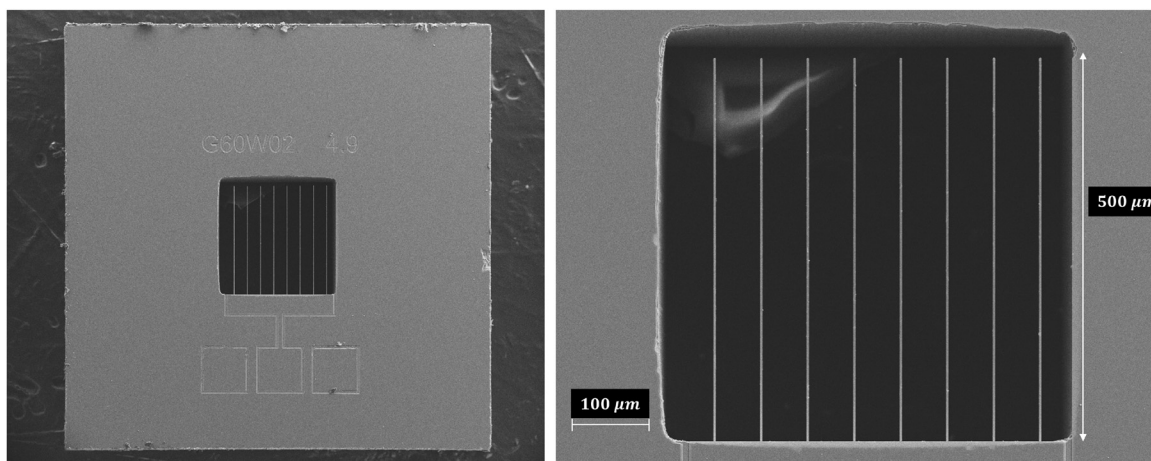


FIG. 1. Microfabricated cantilever beams fabricated on a silicon chip. The cantilever beams are over a central square through-hole. The dimensions of the chip are  $2 \text{ mm} \times 2 \text{ mm} \times 0.5 \text{ mm}$ . The central through-hole is  $500 \mu\text{m} \times 500 \mu\text{m} \times 500 \mu\text{m}$ . The beams are  $480 \mu\text{m}$  long and  $340 \text{ nm}$  thick. Three widths of beams are measured: 2, 3, and  $5 \mu\text{m}$ . The beams are made of a sandwich of silicon nitride-polysilicon-silicon nitride.

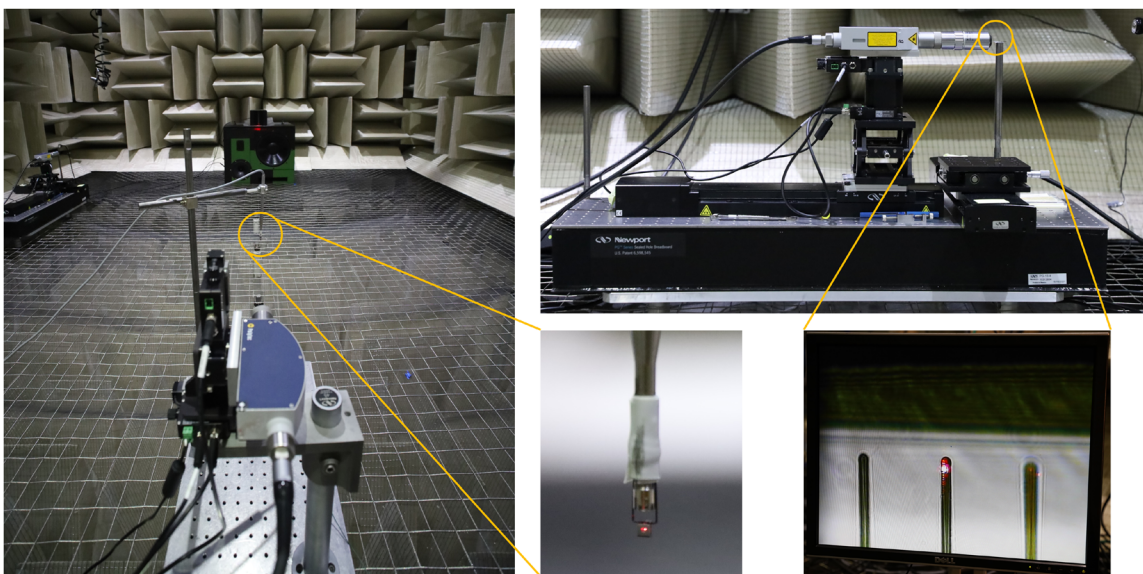


FIG. 2. (Color online) Experimental setup of the measurement. (a) Acoustic response setup, (b) thermal noise measurement setup, and (c) mounting of the test sample are shown. The motion of the beam is measured by the laser doppler vibrometer (Polytec OFV-534). The laser is placed at a distance to avoid acoustic reflection for the acoustic response measurement and placed close to test object with a 100× close-up lens for maximum signal to noise ratio. For stimulation, step sinusoidal signals are used to acquire the acoustical frequency response while eliminating the acoustical reflection and uncorrelated noise. The reference microphone (B & K type 4138 1/8 in.) is placed adjacent to the chip to measure the sound pressure for acoustic particle velocity calculation. National Instruments PXI 1033 data acquisition system is used for data acquisition. Laser is positioned on the tip of the beam.

The results of Figs. 3 and 4 are used in Fig. 5 to show the predicted and measured power spectral densities of the acoustic pressure-referred noise for these beams. The results again show good agreement between measurements and predictions over much of the audible range of frequencies. The predicted and measured beam velocities obtained from measurements and the COMSOL finite element model are in much closer agreement than those of the analytical model. This difference is likely due to the fact that the COMSOL

result more accurately accounts for the actual viscous acoustic flow within the chip than is assumed in the analytical model. In any case, calculated results and measured results show that changes in the beam width do not have a significant effect on the results.

Figure 5 leads us to conclude that at least for this range of widths, the width of each beam is not a strong parameter in determining its performance in responding to sound. This insensitivity to mechanical parameters can be extremely

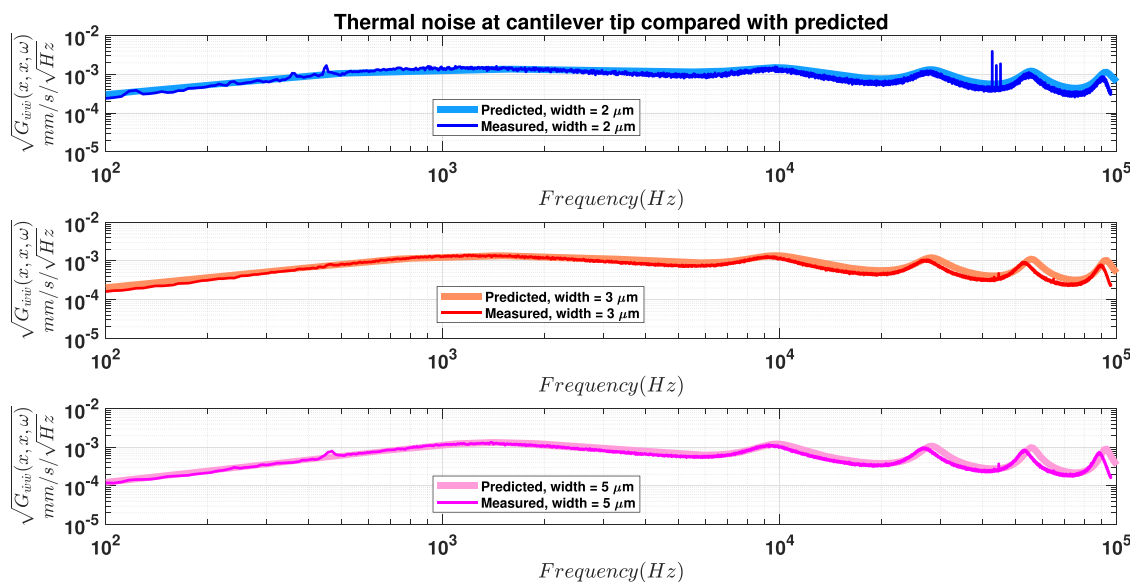


FIG. 3. (Color online) Measured and predicted thermal noise of the beams are in close agreement. Measured and predicted power spectral density of the random response to thermal-mechanical noise are shown for thin micro-cantilever beams with different widths of 2, 3, and 5  $\mu\text{m}$ . Note that the square root of the single-sided velocity power spectral densities,  $\sqrt{G_{\dot{w}i\dot{w}}(x, x, \omega)}$ , are plotted, and  $G_{\dot{w}i\dot{w}}(x, x, \omega) = 4\pi S_{\dot{w}i\dot{w}}(x, x, \omega)$  (Miles, 2020). The results are displayed for the free end of the beam,  $x = l$ .

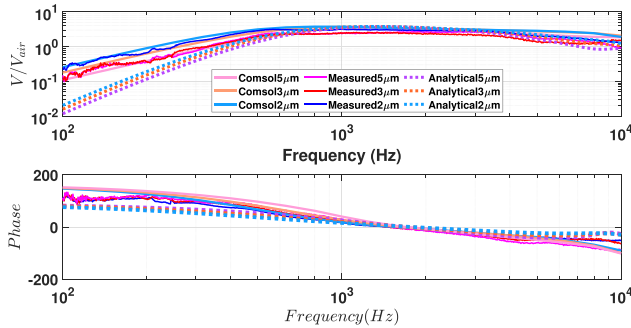


FIG. 4. (Color online) Acoustic frequency response of thin micro-cantilever beams with different widths. The acoustical frequency response of the beams is measured in the anechoic chamber using step sinusoidal pure tone and narrow band least square curve fitting. The results are displayed for the free end of the beam,  $x = l$ . The results obtained using the three methods show that changing the beam width does not significantly affect the results.

beneficial in a design because controlling design parameters in bulk manufacturing can be a vexing challenge and adds considerable expense. It is a remarkable property of viscous fluids that when they interact with sufficiently small, compliant, solid structures, fine geometric details of the structures tend to not impact their overall flow-induced motion.

In addition to examining the effect of beam width on the pressure-referred thermal noise, the effect of changing beam length was also examined. Measurements were performed on beams having lengths of  $L = 500, 480, 446, 396,$  and  $171 \mu\text{m}$ . The lengths and widths of these beams are quite small relative to the wavelength of sound in the audible frequency range.

The predicted and measured power spectral densities of the acoustic pressure-referred noise of different length beams depicted in Fig. 8 are calculated from the results of Figs. 6 and 7. Like beams with different widths, the results,

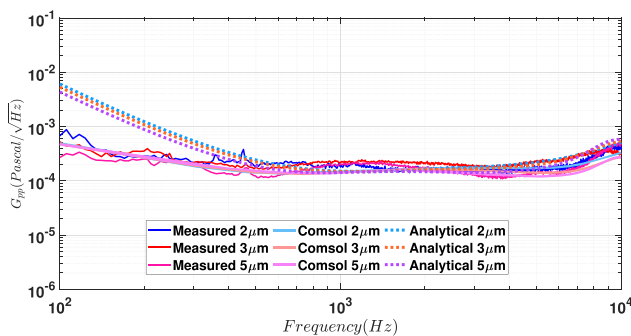


FIG. 5. (Color online) The pressure-referred thermal noise of the beams is not a strong function of the beam width. The pressure-referred noise obtained using a COMSOL model is in close agreement with measured results and nearly independent of frequency over a significant range of audible frequencies for the range of beam widths examined here. The analytical result,  $S_{pp\text{thermal}}$ , as calculated in Eq. (43) is shown to depart from those obtained by measurements, particularly at the lower frequencies. This may be because of the difficulty of estimating the viscous flow within the chip in which the beams are fabricated. In each case, however, the beam width does not appear to be a significant parameter in determining the results. The results are shown for the free end of the beam,  $x = l$ . Note, again, that the square root of the single-sided velocity power spectral densities,  $\sqrt{G_{pp}(l, \omega)}$ , are plotted, and  $G_{pp}(l, \omega) = 4\pi S_{pp}(l, \omega)$ .

again, show good agreement between measurements and predictions over much of the audible range of frequencies for all of the lengths investigated here. The predicted and measured beam velocities obtained from measurements and the COMSOL finite element model are in much closer agreement than those of the analytical model at the lower frequencies. This is, once more, probably because the finite element model more accurately accounts for the influence of the chip geometry on the acoustic flow near the beam. Calculated and measured results show that changes in the beam lengths do not have a dramatic effect on the results. Once again, Fig. 8 leads us to the conclusion that changes in the mechanical parameters of each beam do not have a strong influence on its performance in responding to sound.

### VII. THE PRESSURE-REFERRED THERMAL NOISE IS INVERSELY PROPORTIONAL TO DAMPING FOR THESE ACOUSTIC FLOW-SENSING BEAMS

The results displayed in Figs. 3–8 indicate that the analytical model for the pressure-referred noise of these thin beams does a reasonable job of accounting for the viscous forces applied to the beam by the air. As mentioned above, we would like to explore how the pressure-referred noise depends on the viscous damping of these beams. Here, we would like to avoid the single-mode assumption used to derive Eqs. (35) and (45). To accomplish this, we consider the pressure-referred noise of one beam having a width of  $2 \mu\text{m}$  at a single frequency of 1 kHz. The dimensions and material properties of the beam are held fixed, but the calculations are performed for a range of values of the viscosity of the fluid (air). Increasing the viscosity will, of course, increase the damping constant,  $C$ , depending on the details of the viscous flow around the beam, as examined in Miles (2020). The results of this numerical study presented in Fig. 9 show that the pressure-referred noise clearly decreases significantly as the viscous damping constant,  $C$ , increases. The noise appears to be proportional to the inverse of  $C$  as expected by examining the leading term in Eq. (44).

Although these numerical results were obtained by artificially modifying the fluid viscosity, they suggest that for an acoustic sensor that detects fluid motion rather than sound pressure, it is very beneficial to seek designs of the sensing structure that maximize the effective damping constant,  $C$ . This will minimize the influence of thermal noise on the structure’s motion.

### VIII. DISCUSSION AND CONCLUSIONS

This study has been motivated by a desire to consider methods of creating microphones based on the detection of the acoustic particle velocity rather than the fluctuating sound pressure, as is used in essentially all current microphone designs. Countless animals hear sound by detecting the motion of thin hair-like structures that are driven by viscous forces due to the sound-induced motion of air. An important step in contemplating engineered designs based on this approach is to consider in what way the essential

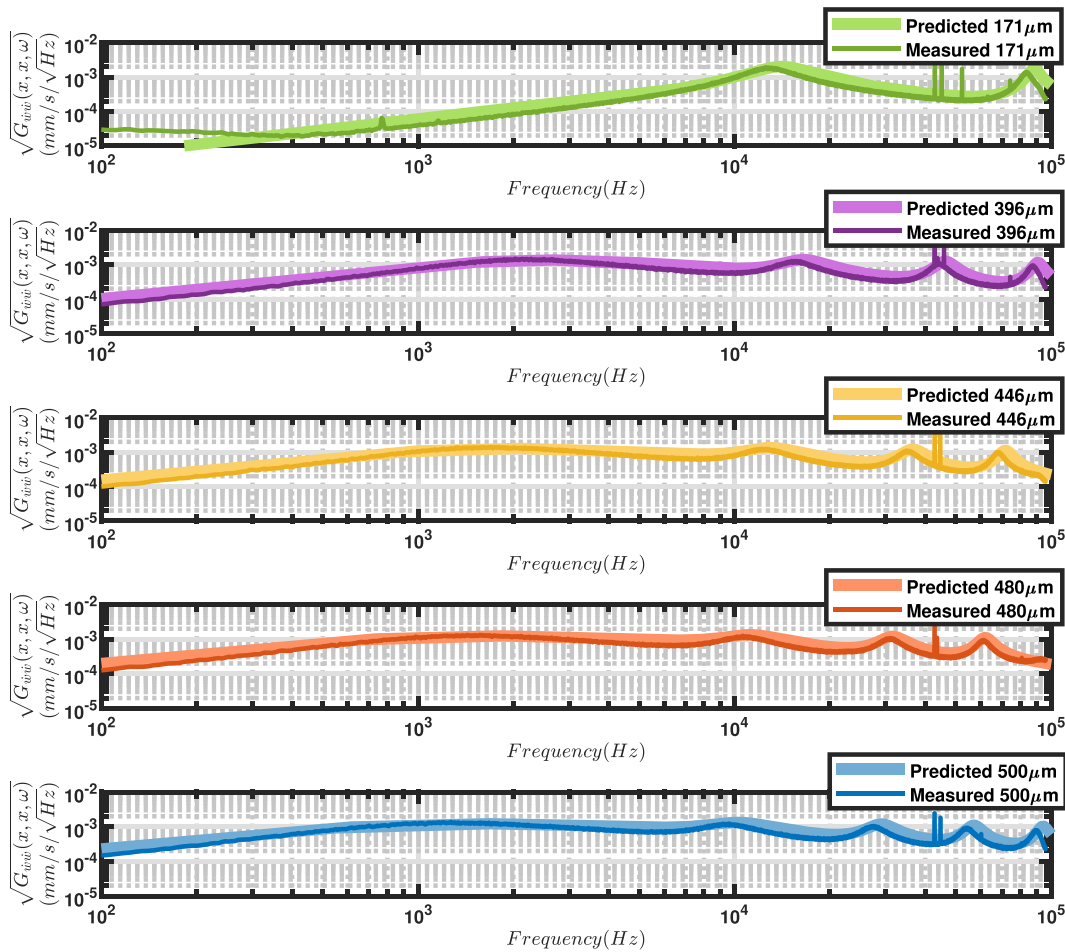


FIG. 6. (Color online) Measured and predicted power spectral densities of the random response to thermal-mechanical noise of thin micro-cantilever beams with different lengths of 171, 396, 446, 480, and 500  $\mu\text{m}$  are in close agreement. The results are displayed for the free end of the beam,  $x = l$ .

design parameters influence how quiet a sound a flow-sensing microphone could detect. Because we have well over 100 years of design experience in pressure-sensing microphones, it is well known that as the pressure-sensing diaphragm becomes smaller, thermal noise from the surrounding gas can adversely affect the signal. The influence of thermal noise of pressure-sensing microphones is reduced by making the diaphragm larger and minimizing sources of energy dissipation (i.e., damping). When the sensing structure is intended to detect acoustic particle velocity (i.e., flow) rather than pressure, it is not obvious how the dominant parameters of the design impact the influence of thermal noise on the structure’s motion relative to the detected sound.

In creating any system for detecting sound, it is important to carefully consider the fact that in a traveling sound wave, there are fluctuating pressures that propagate in space and as a result, portions of the medium can experience unbalanced forces on opposing sides of any small volume. The unbalanced fluctuating forces result in fluctuating motion of the medium. Detecting that motion can be an alternative to attempting to detect the forces or sound pressure. It is also important to note that the medium is composed of vast numbers of individual particles or molecules,

which all exhibit uncorrelated, random motion. The detection system must, somehow, respond to the spatial average acoustic fluctuations of the ensemble rather than to the individual particles.

Because sound in air involves extremely small motions and forces, any mechanical structure intended to move with the air should be as compliant and have as little mass as possible (Miles, 2020). This is surely true whether the aim is to detect pressure or motion. In systems for measuring sound underwater, it can be advantageous to achieve neutral buoyancy by using an enclosed air-filled chamber (Ivancic *et al.*, 2023). It would be an interesting challenge to apply this idea when the medium is a gas such as air.

In addition to a focus on devices that are highly compliant and have minimal inertia, the importance of minimizing overall device size has dominated microphone research, owing to the related reduction in production cost. When the size of a solid object (such as a diaphragm, beam, hair, or fiber) interacting with a fluid, such as air, becomes sufficiently small, viscous forces of the fluid can increase in importance relative to those caused by pressure. When the size of the object is microscopic, viscous forces can dominate over forces that we usually encounter such as pressure and gravity; small dust particles float in the air while large

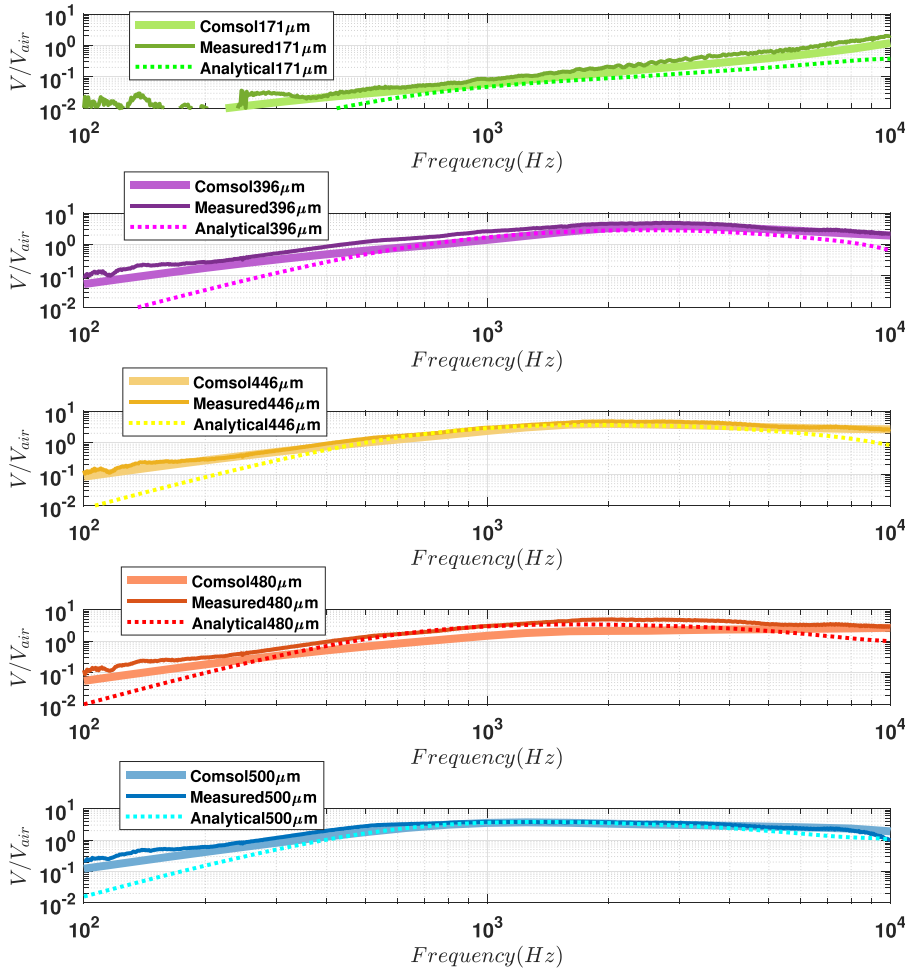


FIG. 7. (Color online) Measured and predicted acoustic response of thin micro-cantilever beams with different lengths of 171, 396, 446, 480, and 500  $\mu\text{m}$ . The results are displayed for the free end of the beam,  $x=l$ . The results obtained using the three methods show that changing the beam length does not significantly affect the results.

objects certainly do not. The importance of viscosity relative to pressure and pressure gradients in small acoustic sensors deserves more attention (Miles and Zhou, 2018; Zhou and Miles, 2017).

The sound-induced motion of a solid object, such as a beam or an animal’s sensory hair, could be the result of differences in pressure on its opposing sides in a traveling sound wave or it could be the result of viscous forces in the moving fluid. Of course, the air is moving because of pressure gradients, therefore, it can be somewhat unclear

whether to attribute the object’s motion to viscous forces or simple pressure gradients. One way to examine this might be to remove viscosity and see what difference it makes on the resulting motion. Although this is straightforward in a

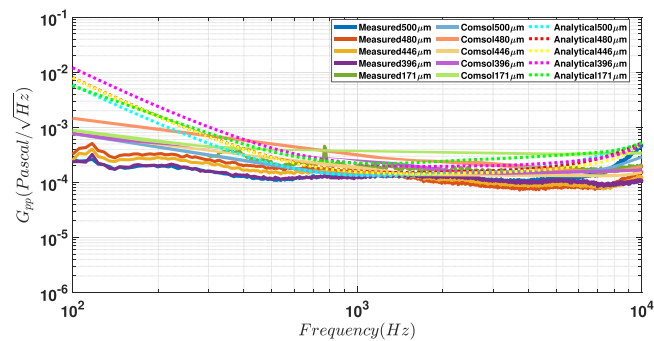


FIG. 8. (Color online) The beam length does not have a marked influence on the pressure-referred noise. Measured and predicted pressure-referred noise of thin micro-cantilever beams with different lengths reasonably agree over much of the audible range.

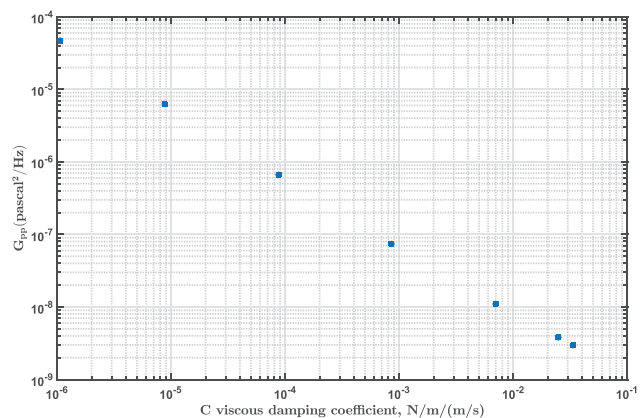


FIG. 9. (Color online) Increasing the viscous damping coefficient per unit length reduces the pressure-referred thermal noise. Power spectral density of the pressure-referred thermal noise of a thin micro-cantilever beam having a width of 2  $\mu\text{m}$  versus the viscous damping coefficient per unit length. The results are displayed for a frequency of 1 kHz. The calculations were performed using a range of values of the air viscosity which caused the viscous damping coefficient to vary over the range depicted. These results show that the pressure-referred noise is proportional to the inverse of the viscous damping coefficient as indicated in Eq. (44).

numerical model, it is not a simple matter to accomplish this in an experiment. Numerical results that we have obtained indicate that when viscosity is dramatically reduced, the sound-induced motion of these beams is substantially less. Based on our numerical results, we have concluded that viscosity plays a dominant role for these beams.

The focus of the present study is on relatively simple candidate structures that could be considered in an acoustic flow-sensing microphone. Of course, as is clear by the variety of forms used by animals for detecting acoustic flow, there are countless possible engineered designs that could be considered. We have concentrated on a rather simple candidate design consisting of a thin, narrow, cantilever beam. The properties of the beam are chosen such that its motion due to a traveling acoustic wave resembles the acoustic particle velocity. Analytical models of the response to sound and the response to random thermal noise are in close agreement with experimental results.

One of the main findings in this study is that the sound-induced motion and the effective sound pressure that elicits the same response as the thermal noise excitation (i.e., the pressure-referred noise) is not a strong function of the width and length of the beams. The beams chosen here are quite narrow (from 2 to 5  $\mu\text{m}$  in width). This suggests that for sufficiently thin sensing structures, geometric details are not particularly important. Not needing to worry extensively about dimensional tolerances (and, perhaps, material properties) can lead to significant benefits when fabricating devices.

Another conclusion of this study is that it is very beneficial to seek designs that maximize the effective viscous damping coefficient that determines the viscous force on the structure resulting from the relative velocity between the structure and fluid. The dependence of the sound pressure-referred noise on the viscous damping can be observed in the analytical model and is apparent in the numerical results. Whereas the present study has focused on fairly simple cantilever beams as the sensing structure, many other geometries could be considered, having enhanced surface area that enables them to achieve higher viscous damping coefficients.

Although our attention here has been focused on an examination of thermal noise in microphones designed to be driven by viscous flow, the transition from sensing pressure to sensing flow will introduce myriad other important considerations. One important aspect is that flow often depends substantially on the boundary conditions near the sensing structure; fluid flow can be very strongly dependent on position while pressure tends to be less so. The enclosure or package then must be designed carefully. With proper design, the surrounding structure can provide an increase in flow velocity which could enhance performance significantly.

By focusing solely on thermal noise in the present study, we have avoided the very difficult issue of selecting the most effective means of transduction. Achieving an electronic readout, obviously, is an essential task which, admittedly, can be daunting. In the simple beams examined here,

transduction could be achieved using capacitance, strain, or optical methods, which have been used successfully in pressure microphones. Capacitive transduction may require a departure from the common parallel plate design but might take the form of interdigitated fingers or other less common electrodes. Because the structure should be as compliant as possible and have minimal mass, the transduction scheme should be designed to apply as little force to the structure as possible. An attempt at a capacitive sensing system that is designed to achieve this has been described previously (Miles, 2018).

## ACKNOWLEDGMENTS

Research reported in this publication was supported by the National Institute on Deafness and Other Communication Disorders of the National Institutes of Health under Award No. R01DC017720 to R.M. The authors thank Soundskrit, Inc. (Montreal, Canada) for providing the microfabricated beams displayed in Fig. 1.

## AUTHOR DECLARATIONS

### Conflict of Interest

The authors have no conflicts to disclose.

## DATA AVAILABILITY

The data that support the findings of this study are available within the article.

- Asadnia, M., Kottapalli, A. G. P., Karavitaki, K. D., Warkiani, M. E., Miao, J., Corey, D. P., and Triantafyllou, M. (2016). "From biological cilia to artificial flow sensors: Biomimetic soft polymer nanosensors with high sensing performance," *Sci. Rep.* **6**(1), 32955.
- Bezares-Calderón, L. A., Berger, J., and Jékely, G. (2020). "Diversity of cilia-based mechanosensory systems and their functions in marine animal behaviour," *Philos. Trans. R. Soc. B* **375**(1792), 20190376.
- Bhiladvala, R. B., and Wang, Z. J. (2004). "Effect of fluids on the  $Q$  factor and resonance frequency of oscillating micrometer and nanometer scale beams," *Phys. Rev. E* **69**(3), 036307.
- Bidkar, R. A., Tung, R. C., Alexeenko, A. A., Sumali, H., and Raman, A. (2009). "Unified theory of gas damping of flexible microcantilevers at low ambient pressures," *Appl. Phys. Lett.* **94**(16), 163117.
- Blom, F. R., Bouwstra, S., Elwenspoek, M., and Fluitman, J. H. J. (1992). "Dependence of the quality factor of micromachined silicon beam resonators on pressure and geometry," *J. Vac. Sci. Technol. B* **10**(1), 19–26.
- Butt, H.-J., and Jaschke, M. (1995). "Calculation of thermal noise in atomic force microscopy," *Nanotechnology* **6**(1), 1.
- Chon, J. W., Mulvaney, P., and Sader, J. E. (2000). "Experimental validation of theoretical models for the frequency response of atomic force microscope cantilever beams immersed in fluids," *J. Appl. Phys.* **87**(8), 3978–3988.
- de Bree, H.-E. (2003). "An overview of microflow technologies," *Acta Acust. Acust.* **89**(1), 163–172.
- Dijkstra, M., Van Baar, J., Wiegerink, R. J., Lammerink, T. S., De Boer, J., and Krijnen, G. J. (2005). "Artificial sensory hairs based on the flow sensitive receptor hairs of crickets," *J. Micromech. Microeng.* **15**(7), S132.
- Fellgett, P. (1987). "Thermal noise limits of microphones," *J. Inst. Electron. Radio Eng. UK* **57**(4), 161–166.
- Forbes, G. (1887). "III. A thermal telephone transmitter," *Proc. R. Soc. London* **42**(251–257), 141–142.
- Gabrielson, T. (1993). "Mechanical-thermal noise in micromachined acoustic and vibration sensors," *IEEE Trans. Electron Devices* **40**(5), 903–909.

- ISO 3745 (2003). "Acoustics – Determination of sound power levels of noise sources using sound pressure – Precision methods for anechoic and hemi-anechoic rooms" (International Organization for Standardization, Geneva, Switzerland).
- Ivancic, J., Catterlin, J., Karunasiri, G., and Alves, F. (2023). "MEMS directional underwater acoustic sensor operating in near neutral buoyancy configuration," in *2023 IEEE International Symposium on Inertial Sensors and Systems (INERTIAL)*, 28–31 March, Lihue, HI (IEEE, New York), pp. 1–4.
- Jandak, M., Neuzil, T., Schneider, M., and Schmid, U. (2016). "Investigation on different damping mechanisms on the  $Q$  factor of mems resonators," *Procedia Eng.* **168**, 929–932.
- Julius, W., and Olson, H. F. (1932). "Sound pick-up device," U.S. patent 1,892,645.
- Kittel, C. (1958). *Elementary Statistical Physics* (Wiley, New York).
- Krijnen, G. J., Dijkstra, M., van Baar, J. J., Shankar, S. S., Kuipers, W. J., de Boer, R. J., Altpeter, D., Lammerink, T. S., and Wiegerink, R. (2006). "MEMS based hair flow-sensors as model systems for acoustic perception studies," *Nanotechnology* **17**(4), S84.
- Lai, J., Karimi, M., and Miles, R. (2022). "Methods for accurate acoustic characterization with ultra-low noise and minimal effect from reflection wave," *J. Acoust. Soc. Am.* **152**(4), A194.
- Miles, R. (2018). "A compliant capacitive sensor for acoustics: Avoiding electrostatic forces at high bias voltages," *IEEE Sens. J.* **18**, 5691–5698.
- Miles, R. (2019). "Most animals hear acoustic flow instead of pressure; we should too," *J. Acoust. Soc. Am.* **145**(3), 1698.
- Miles, R., and Zhou, J. (2018). "Sound-induced motion of a nanoscale fiber," *J. Vib. Acoust.* **140**(1), 011009.
- Miles, R. N. (2020). *Physical Approach to Engineering Acoustics* (Springer, New York).
- Sader, J. E. (1998). "Frequency response of cantilever beams immersed in viscous fluids with applications to the atomic force microscope," *J. Appl. Phys.* **84**(1), 64–76.
- Stokes, G. G. (1851). "On the effect of the internal friction of fluids on the motion of pendulums," *Trans. Cambridge Philos. Soc.* **IX**, 8.
- Sumali, H., and Carne, T. G. (2007). "Air damping on micro-cantilever beams," Sandia National Laboratory Report No. SAND2007-6842C (SNL-NM, Albuquerque, NM).
- Tao, J., and Yu, X. B. (2012). "Hair flow sensors: From bio-inspiration to bio-mimicking—A review," *Smart Mater. Struct.* **21**(11), 113001.
- Tucker, W. S., and Paris, E. T. (1921). "XI. A selective hot-wire microphone," *Philos. Trans. R. Soc. London, Ser. A* **221**(582-593), 389–430.
- Van Baar, J., Dijkstra, M., Wiegerink, R., Lammerink, T., De Boer, R., and Krijnen, G. (2005). "Arrays of cricket-inspired sensory hairs with capacitive motion detection," in *18th IEEE International Conference on Micro Electro Mechanical Systems, MEMS 2005*, 30 January-3 February 2005, Miami Beach, FL (IEEE, New York), pp. 646–649.
- Verbridge, S. S., Ilic, R., Craighead, H. G., and Parpia, J. M. (2008). "Size and frequency dependent gas damping of nanomechanical resonators," *Appl. Phys. Lett.* **93**(1), 013101.
- Zalalutdinov, M., Photiadis, D., Szymczak, W., McMahon, J., Bucaro, J., and Houston, B. (2017). "Mesh-type acoustic vector sensor," *J. Appl. Phys.* **122**(3), 034504.
- Zhou, J., Lai, J., Menda, G., Stafstrom, J. A., Miles, C. I., Hoy, R. R., and Miles, R. N. (2022). "Outsourced hearing in an orb-weaving spider that uses its web as an auditory sensor," *Proc. Natl. Acad. Sci. U.S.A.* **119**(14), e2122789119.
- Zhou, J., Li, B., Liu, J., Jones, W. E., Jr., and Miles, R. N. (2018). "Highly-damped nanofiber mesh for ultrasensitive broadband acoustic flow detection," *J. Micromech. Microeng.* **28**(9), 095003.
- Zhou, J., and Miles, R. N. (2017). "Sensing fluctuating airflow with spider silk," *Proc. Natl. Acad. Sci. U.S.A.* **114**, 12120–12125.